1521-0111/99/1/49–59$35.00
MOLECULAR PHARMACOLOGY

https://doi.org/10.1124/molpharm.120.000079
Mol Pharmacol 99:49–59, January 2021



# Characterization of Vixotrigine, a Broad-Spectrum Voltage-Gated Sodium Channel Blocker[S]

Christopher A Hinckley, Yuri Kuryshev, Alissende Sers, Alexander Barre, Bruno Buisson, Himanshu Naik, and Mihaly Hajos1

*Biogen, Cambridge, Massachusetts (C.A.H., H.N.); Charles River Laboratories Cleveland, Inc., Cleveland, Ohio (Y.K.); Neuroservice, Aix-en-Provence, France (A.S., A.B., B.B.); and Department of Comparative Medicine, Yale University, New Haven, Connecticut (M.H.)*

Received June 8, 2020; accepted October 15, 2020

## ABSTRACT

Voltage-gated sodium channels (Navs) are promising targets for analgesic and antiepileptic therapies. Although specificity between Nav subtypes may be desirable to target specific neural types, such as nociceptors in pain, many broadly acting Nav inhibitors are clinically beneficial in neuropathic pain and epilepsy. Here, we present the first systematic characterization of vixotrigine, a Nav blocker. Using recombinant systems, we find that vixotrigine potency is enhanced in a voltage- and use-dependent manner, consistent with a state-dependent block of Navs. Furthermore, we find that vixotrigine potently inhibits sodium currents produced by both peripheral and central nervous system Nav subtypes, with use-dependent $IC_{50}$ values between 1.76 and 5.12 μM. Compared with carbamazepine, vixotrigine shows higher potency and more profound state-dependent inhibition but a similar broad spectrum of action distinct from Nav1.7- and Nav1.8-specific blockers. We find that vixotrigine rapidly inhibits Navs and prolongs recovery from the fast-inactivated state. In native rodent dorsal root ganglion sodium channels, we find that vixotrigine shifts steady-state inactivation curves. Based on these results, we conclude that vixotrigine is a broad-spectrum, state-dependent Nav blocker.

## SIGNIFICANCE STATEMENT

Vixotrigine blocks both peripheral and central voltage-gated sodium channel subtypes. Neurophysiological approaches in recombinant systems and sensory neurons suggest this block is state-dependent.

## Introduction

Pathologically elevated neural activity underlies common central nervous system (CNS) and peripheral nervous system (PNS) diseases, including epilepsy and neuropathic pain. Inhibitors of voltage-gated sodium channels (Navs) are commonly used treatments for these diverse conditions; for example, the anticonvulsant carbamazepine is indicated for many types of epilepsy and is a first-line treatment of trigeminal neuralgia (Wiffen et al., 2011).

Based on expression patterns in nociceptive neurons, a variety of Navs have been implicated in neuropathic pain. Nav1.3, which is highly expressed in development, is upregulated after injury and inflammation (Waxman et al., 1994; He et al., 2010). Nav1.7, 1.8, and 1.9 are enriched in nociceptive neurons and serve to amplify subthreshold depolarizations, set action-potential thresholds, and drive the action-potential upstroke (Bennett et al., 2019).

Genetic evidence has identified gain-of-function mutations in Nav1.7 as causative in rare forms of pain hypersensitivity (Cummins et al., 2004; Yang et al., 2004). This result generated significant interest in the development of Nav1.7-specific blockers for analgesia; however, subsequent genetic and physiologic studies have identified both gain- and loss-of-function mutations in Nav1.7, 1.8, and 1.9 that lead to hypersensitivity and insensitivity to pain. Similarly, mutations in Nav1.6 and 1.2 are associated with epilepsy (Veeramah et al., 2012; Howell et al., 2015). The potential to specifically inhibit genetically validated Nav pain and epilepsy targets while avoiding cardiac and skeletal muscle effects of Nav has generated interest in developing Nav subtype–selective inhibitors with efficacy in both the CNS and the PNS. Although these efforts are hampered by the high homology between Nav subtypes, some Nav subtype–selective small molecules have been reported, as have selective peptide

**Primary laboratory of origin:** Charles River Laboratories, Cleveland, OH (for Y.K.).
The study was funded by Biogen.
C. Hinckley, M. Hajos, and H. Naik are/were employees of and own stock/stock options in Biogen. Y. Kuryshev, A. Sers, A. Barre, and B. Buisson have no conflicts of interest to declare.
[1]Current affiliation: Department of Comparative Medicine, Yale University, New Haven, Connecticut.
https://doi.org/10.1124/molpharm.120.000079.
[S] This article has supplemental material available at molpharm.aspetjournals.org.

**ABBREVIATIONS:** CHO-T, CHO tetracycline-inducible; CNS, central nervous system; CRL, Center for Research Libraries; DRG, dorsal root ganglion; FDA, Food and Drug Administration; HB-PS, HEPES-buffered physiological saline; HBSS, Hanks' balanced salt solution; HEK, human embryonic kidney; IWB, IonWorks Barracuda; Nav, voltage-gated sodium channel; NPC, Nanion patch clamp; PNS, peripheral nervous system; SP384PE, SyncroPatch 384PE; TP, test pulse.

toxins (Jarvis et al., 2007; Alexandrou et al., 2016; Wu et al., 2018).

Despite the promise of subtype-selective inhibition, a variety of broadly acting Nav compounds are in clinical use as analgesics, antiepileptics, and local anesthetics. One example is carbamazepine, a nonselective Nav inhibitor commonly used in trigeminal neuralgia and, less frequently, in epilepsy (Cruccu et al., 2008). An alternative to strict subtype selectivity is state-dependent antagonism, in which a compound preferentially inhibits the channel in its postdepolarization inactivated states, which are enriched in hyperactive or tonically depolarized neurons (Ichikawa et al., 2001). Hyperactive sensory neurons are a hallmark of neuropathic pain (Boucher et al., 2000), suggesting state-dependent Nav blockers will preferentially impact these cells. Likewise, unique state-dependent properties have been proposed for the antiepileptic compound lacosamide, which preferentially binds to slow-inactivated channel states that accumulate after prolonged depolarizations occurring during epileptiform activity (Niespodziany et al., 2013).

Although mechanistically differentiating selective and broad-spectrum Nav blockers is conceptually straightforward, complex functional measurements of ion channel behavior are highly sensitive to experimental protocols. This is particularly relevant for state-dependent properties, for which specific voltage protocols are used to modulate channel states and, thus, the absolute potencies of test compounds. Therefore, Nav blockers are best described with a range of potency values reflecting different experimental protocols, complicating the comparison of results between studies.

Here, we present the first systematic electrophysiological selectivity and mechanism-of-action study of vixotrigine (formerly GSK1014802, CNV1014802, raxatrigine, BIIB074). Vixotrigine, which is in development for neuropathic pain conditions including small fiber neuropathy and trigeminal neuralgia, has been reported as a state-dependent Nav blocker; however, the molecule has been alternatively presented as a Nav1.7-selective or Nav1.7-nonselective compound (Deuis et al., 2016; Hesselink, 2017; Zakrzewska et al., 2017). Using recombinant sodium channels and rodent dorsal root ganglion (DRG) neurons, we show that vixotrigine blocks sodium channels in a voltage- and use-dependent manner. In contrast to reported subtype-selective compounds, we show that vixotrigine inhibits a spectrum of Nav subtypes. Mechanistically, we distinguish vixotrigine from clinically relevant broad-spectrum Nav compounds based on slow- and fast-inactivation kinetic profiles. The broad spectrum, mechanism of action, and potency of vixotrigine suggest therapeutic potential for a variety of indications driven by pathologically elevated neural activity.

## Materials and Methods

**Recombinant Nav1.x Cell Lines.** Cell lines stably expressing human Nav1.1 [Chinese hamster ovary tetracycline-inducible (CHO-T) cells; American Type Culture Collection (Manassas, VA); SCN1A; cat. no. CT6178; Center for Research Libraries (CRL)]; human Nav1.2 (CHO-T; SCN2A; cat. no. CT6010; CRL); human Nav1.3 (CHO-T; SCN3A; cat. no. CT6157; CRL); human Nav1.4 (CHO; SCN4A; cat. no. CT6005; CRL); human Nav1.5 (CHO; SCN5A; cat. no. CT6007; CRL); human Nav1.6 (CHO-T; SCN8A; cat. no. CT6158; CRL); human Nav1.7 (CHO-T; SCN9A; cat. no. CT6003; CRL); human Nav1.8/$\beta$3 (CHO-T; SCN10A/SCN3B; cat. no. CT6011; CRL); rat Nav1.7 [human embryonic kidney (HEK) 293 cells; ATCC; SCN9A; cat. no. CT6013; CRL]; and rat Nav1.8/$\beta$3 (CHO-T; SCN10A/SCN3B; cat. no. CT6014; CRL) ion channels were constructed as described previously (Wible et al., 2008). The cDNA sequences of the Navs are identical to the following reference sequences: NM_006920.3 (human Nav1.1), NM_001040142.1 (human Nav1.2), NM_001081677.1 (human Nav1.3), NM_000334.4 (human Nav1.4), NM_000335.4 (human Nav1.5), NM_014191 (human Nav1.6), NM_002977.3 (human Nav1.7), NM_006514.1 (human Nav1.8), NM_018400.3 (human $\beta$3), NM_133289.1 (rat Nav1.7), NM017247.1 (rat Nav1.8), and NM_139097.3 (rat $\beta$3). CHO cells were maintained in 100-mm cell culture dishes in Ham's F-12 CHO media (ATCC) supplemented with 10% fetal bovine serum (MilliporeSigma, St. Louis, MO), 100 U/ml of penicillin G sodium, 100 mg/ml of streptomycin sulfate, and the appropriate selection antibiotics. HEK293 cells were maintained in 100-mm cell culture dishes in Dulbecco's modified Eagle's medium/F-12/G media (ATCC) supplemented with 10% fetal bovine serum (MilliporeSigma), 100 U/ml of penicillin G sodium, 100 mg/ml of streptomycin sulfate, and the appropriate selection antibiotics. The absence of mycoplasma species in all cell lines was confirmed with the MycoAlert Kit (Lonza Rockland, Inc.).

For experiments, the cells were passed in selection antibiotic–free medium. Expression was induced with tetracycline 16–24 hours before recording. Cell density was 50%–70% confluent at the time of harvesting. Cells were harvested by washing twice with Hanks' balanced salt solution (HBSS) and treating with Accutase (Innovative Cell Technologies, San Diego, CA) solution for 20 minutes. Detached cells were transferred in a 15-ml conical tube and resuspended with the addition of 10 ml of HBSS. Then the cells were pelleted at 500*g* for 2.0 minutes, the supernatant was removed, and the cell pellet was resuspended in 10 ml of HBSS. The cell suspension was centrifuged again at 500*g* for 2.0 minutes, and the supernatant was removed. Finally, the cell pellet was resuspended in 5 ml of HEPES-buffered physiologic saline (HB-PS) containing 137 mM NaCl, 4 mM KCl, 1.8 mM $CaCl_2$, 1 mM $MgCl_2$, 10 mM HEPES, and 10 mM glucose (adjusted to pH 7.4 with NaOH), and osmolarity was adjusted to 295 ± 5 mOsm. The final cell dilution was approximately $10^6$ cells/ml.

**Solutions, Test Articles, and Electrophysiological Procedures.** Chemicals used in a solution preparation were purchased from MilliporeSigma and were of American Chemical Society reagent–grade purity or higher. Vixotrigine was produced internally. Stock solutions of test articles were prepared in DMSO and stored frozen. For experiments, test article concentrations were prepared fresh daily by diluting stock solutions into extracellular solutions (HB-PS buffer) supplemented with 2 mM $CaCl_2$. The final solution composition was 137 mM NaCl, 4 mM KCl, 3.8 mM $CaCl_2$, 1 mM $MgCl_2$, 10 mM HEPES, and 10mM glucose (adjusted to pH 7.4 with NaOH). All test and control solutions contained 0.3% DMSO.

Six test articles were used: PF-05089771 (4-[2-(3-Amino-1*H*-pyrazol-4-yl)-4-chlorophenoxy]-5-chloro-2-fluoro-*N*-4-thiazolylbenzenesulfonamide tosylate, selective Nav1.7 inhibitor), A-803467 (5-(4-Chlorophenyl)-*N*-(3,5-dimethoxyphenyl)-2-furancarboxamide, selective Nav1.8 inhibitor), vixotrigine, lacosamide, lamotrigine, and carbamazepine, with test concentrations ranging from 0.03 to 1000 μM. Lidocaine was used as a positive control at concentrations ranging from 0.3 to 3000 μM. The test article formulations were prepared in 384-well compound plates using an automated liquid handling system (Integra Assist Plus, Integra Biosciences, Hudson, NH).

Recordings were performed on the IonWorks Barracuda (IWB) system (Molecular Devices Corporation, Union City, CA) and the SyncroPatch 384PE (SP384PE) system (Nanion Technologies, Livingston, NJ).

**IWB Patch Clamp, Population Patch-Clamp Mode, and Perforated Patch Whole-Cell Configuration.** The internal HEPES-buffered solution consisted of 90 mM CsF, 50 mM CsCl, 2 mM $MgCl_2$, 2.5 mM EGTA, and 10 mM HEPES (adjusted to pH 7.2 with CsOH).

A stock solution of amphotericin B (perforating agent) was prepared in DMSO (30 mg/ml) and added to the internal solution at a final concentration of 30 μg/ml. The extracellular solution was loaded into the population patch-clamp plate wells (11 μl/well), and a cell suspension was added into the wells (9 μl/well). After establishment of a whole-cell configuration (7-minute perforation), membrane currents were recorded by IWB on-board patch-clamp amplifiers. Test article concentrations were applied to naive cells (four wells per concentration). Each application consisted of the addition of 20 μl of two times concentrated test article solution to the total 40-μl final volume of the extracellular well of the population patch-clamp plate. Duration of exposure to each test article concentration was 5 minutes.

**SP384PE Patch Clamp, Multicell Mode, and Standard Whole-Cell Configuration.** Intracellular solution for the whole-cell recording (the same as for IWB) was loaded into the intracellular compartment of a 384-well Nanion patch clamp (NPC) chip (Nanion Technologies, Munich, Germany). Extracellular HB-PS was loaded into NPC chip wells (80 μl/well). The cell suspension was pipetted into the wells of the NPC (20 μl/well). After establishment of a whole-cell configuration, membrane currents were recorded using patch-clamp amplifiers in the SP384PE system. Test article concentrations were applied to naive cells ($n$ = 4 replicates per concentration). Each application consisted of the addition of 40 μl of two times concentrated test article solution to the total 80-μl final volume of the extracellular well of the NPC chip.

For both systems, duration of exposure to each test article concentration was 5 minutes. The current recordings were performed once before the test article application to the cells (baseline) and once after application of the test article. Similar voltage protocols were used in IWB and SP384PE recordings.

**Automated Patch Clamp: Voltage- and Use-Dependence Protocols.** Sodium currents were evoked with 25-millisecond depolarizing pulses to +10 mV (Nav1.1, 1.2, 1.3, and 1.8) or 0 mV (Nav1.4, 1.5, 1.6, and 1.7). Voltage dependence was examined from holding potentials of –90 and –60 mV (–70 mV for Nav1.5); cells were held at these membrane potentials before and between sweeps. After a 20-millisecond prepulse of –120 mV, cells returned to the holding potential for 40 milliseconds prior to evoking sodium currents. Use-dependent modulation of the sodium currents was examined with a series of 25 pulses at 10 Hz from an interpulse holding potential of –90 or –60 mV (–70 mV for Nav1.5). Voltage protocols were repeated at 0.1 Hz.

**Automated Patch Clamp: Slow- and Fast-Inactivation Protocols.** The onset of slow inactivation was examined with 0-mV voltage pulses between 2.5 and 10,240 milliseconds, followed by a 5-millisecond recovery pulse to –120 mV. Sodium currents were evoked with a 0-mV, 25-millisecond depolarizing pulse. Recovery from slow inactivation was examined after a 1-second, 0-mV conditioning pulse, followed by recovery pulses of –120 mV between 2.5 and 10,240 milliseconds. Recovery from fast inactivation was examined after 10-millisecond, 0-mV conditioning pulses and recovery pulses of –120 mV between 2.5 and 10,240 milliseconds.

**Rodent DRG Isolation and Recording.** Animal experiments were performed in accordance with applicable local guidelines (Animal Facilities agreement A1305534, Animal project agreement 13288-2018022522441658v5 granted to Neuroservice). DRG were dissected from 7- to 10-week-old Sprague-Dawley rats (two female, seven male; obtained from Janvier Laboratories). DRG were collected in cold HBSS-glucose. DRG were treated first for 20 minutes with Collagenase-Dispase solution (2 ml) at 37°C; after that, the solution was removed, and new Collagenase-Dispase solution (2 ml) was added for an additional 20 minutes of enzymatic treatment. DRG were washed twice with prewarmed HBSS-glucose. DRG were resuspended into 1 ml of Neurobasal A medium with B27 supplement, penicillin-streptomycin, and glutamine. A single-cell suspension was obtained by six passages through decreasing needle diameters (21G, 23G, and 26G). Cells were seeded onto a glass coverslip coated with poly-D-Lysine and laminin solutions. After 2 hours, the medium was replaced by fresh B27-supplemented Neurobasal A. DRG neurons were recorded after 21–30 hours in culture. Only neurons ≤25 μm in diameter were targeted for recording. Whole-cell patch-clamp experiments were performed at room temperature in voltage mode using a MultiClamp 700B Amplifier and Axon Digidata 1440A Digitizer (Molecular Devices Corporation). Data were low-pass-filtered at 2 kHz before being sampled at 50 kHz using Clampex 10 software. Patch pipettes were pulled from borosilicate glass capillaries with resistances of 2.5–4 MΩ. Each recorded neuron was validated by using criteria of acceptable maximal leak amplitude (<150 pA) and fluctuation of the Series Resistance (Maximal Series Resistance: 20 MΩ, ΔSeries Resistance < 50%). Raw data were analyzed by using Clampfit 10.3 software and IGOR PRO 6.3 software.

Intracellular solutions contained CsF 140 mM, NaCl 10 mM, $MgCl_2$ 2 mM, $CaCl_2$ 0.1 mM, EGTA 1.1 mM, and HEPES 10 mM, adjusted to pH 7.2 with CsOH. Extracellular solutions contained tetraethylammonium chloride 107 mM, NaCl 33 mM, KCl 3 mM, $CaCl_2$ 1 mM, $MgCl_2$, HEPES 10mM, glucose 10 mM, and $CdCl_2$ 0.1 mM (adjusted to pH 7.3 with NaOH). Activation profiles were generated after a 1-second prepulse of –120 mV. Peak currents were measured during 1-second test pulses between –80 and +80 mV in 5-mV increments. Inactivation profiles were evoked from 1-second conditioning pulses from –120 to +40 mV in 5-mV increments. Sodium currents were evoked by 20-millisecond test pulses to +10 mV. Test articles were applied for 10 minutes.

**Acceptance Criteria.** Individual well data were filtered according to electrical criteria, and the experiments were accepted based on plate-level acceptance criteria. Well acceptance criteria were seal resistance (baseline) ≥ 300 MΩ, current amplitude (baseline) for Nav1.1–1.7 (inward peak current) ≥ 0.5 nA, and Nav1.8 (inward peak current) ≥ 0.2 nA.

Plate acceptance criteria was Z′ factor (assay sensitivity) ≥ 0.4, where Z′ factor for each experiment was calculated as follows:

$$Z' = 1 - ((3 \times \text{SDVC} + 3 \times \text{SDPC}) / \text{ABS}(\text{MeanVC} - \text{MeanPC})),$$

where MeanVC and SDVC were the mean and S.D. values for a vehicle control, and MeanPC and SDPC were the mean and S.D. values for a positive control (3 mM lidocaine).

**Data Analysis.** The experiments performed in this study were exploratory in nature and designed to characterize the properties of vixotrigine and other Nav-blocking compounds. This work did not employ a predefined study design, including sample size determination; as such, reported $P$ values are descriptive (Michel et al., 2020).

For IWB and SP384PE experiments, data analyses were performed using the system operation software. Data were corrected for leak current.

Tonic block was calculated as follows:

$$\%\text{Block (TP1)} = \left(1 - \left(I_{\text{TP1, TA}}/I_{\text{TP1, Baseline}}\right)\right) \times 100\%,$$

where $I_{\text{TP1, Baseline}}$ and $I_{\text{TP1, TA}}$ were the inward peak $Na^+$ currents elicited by the first test pulse (TP1) in control (baseline) and in the presence of a test article, respectively.

Use-dependent block was calculated as follows:

$$\%\text{Block (use dependent)} = \left(1 - \left(I_{\text{TP25, TA}}/I_{\text{TP25, Baseline}}\right)\right) \times 100\%,$$

where $I_{\text{TP25, TA}}$ and $I_{\text{TP25, Baseline}}$ were the inward peak $Na^+$ currents elicited by the TP25 in control (baseline) and in the presence of a test article, respectively.

The data were corrected for rundown:

$$\%\text{Block'} = 100\% - ((\%\text{Block} - \%\text{PC}) \times (100\%/ (\%\text{VC} - \%\text{PC}))),$$

where %VC and %PC were the mean values of the current inhibition with the vehicle and positive controls, respectively. Rundown correction values are included in Supplemental Table 1.

Results for each test article concentration were averaged (3–11 wells per test article concentration combination), and the mean and S.D. values were calculated and used to generate concentration-response curves. $IC_{50}$ was calculated as the concentration of the test article producing half-maximal inhibition with an equation of the following form:

$$\%\ \text{Block} = 100 / \left(1 + \left([\text{Test}] / IC_{50}\right)^{N}\right),$$

where [Test] was the concentration of test article; $IC_{50}$ was the concentration of the test article producing half-maximal inhibition; *N*, the Hill coefficient, equaled 1; and % Block was the percentage of ion channel current inhibited at each concentration of a test article. Nonlinear least-squares fits were solved with the XL*fit* add-in for Excel (Microsoft, Redmond, WA).

For DRG sodium current recordings, the activation profile was determined by plotting the current density as a function of the depolarization step potential. The inactivation profile was determined by plotting the normalized current density as a function of the conditioning voltage step before the constant voltage step. The decrease in current amplitude after test article application was used to calculate the percent block. A two-way analysis of variance measured differences across groups (control to compound application). The Šidák correction for multiple comparisons was used to assess significant differences in evoked currents at each voltage.

## Results

### Voltage Dependence

To assess the mechanism of action of vixotrigine, we examined the voltage dependence of block in recombinant Navs. Depolarizing voltage pulses evoked sodium currents from holding potentials of –90 and –60 mV (or –70 mV for Nav1.5), near the reported resting membrane potential for human DRG neurons (Fig. 1A). Under our experimental conditions, channel availability at depolarized potentials relative to –90 mV were ~95% for Nav1.1, 86.5% for Nav1.2, 89% for Nav1.3, 50.4% for Nav1.4, 75% for Nav1.5, 58% for Nav1.7, and 59% for Nav1.8 (because of technical limitations, Nav1.6 availability was not determined). We note that this voltage protocol may underestimate voltage dependence for compounds with rapid dissociation kinetics relative to the 20-millisecond prepulse. We defined $IC_{50}$ values as the concentration generating 50% inhibition of the current maximum in baseline (drug-free) conditions. For Nav1.7, we found a 3.64-fold shift in $IC_{50}$ value (28 μM at –90 mV to 6.11 μM at –60 mV), indicating a strong voltage dependence of channel inhibition (Fig. 1B). This shift in $IC_{50}$ was also reflected in the maximum current inhibition obtained across our concentration range, with vixotrigine reaching >97% inhibition of the baseline Nav1.7 current from –60 mV, compared with ~80% from –90 mV at our maximum concentration of 100 μM. Next, we compared the voltage dependence of inhibition across a panel of Navs (Fig. 1C). We found that $IC_{50}$ values shifted toward increased potency for Nav1.1–1.7 block, with an average of a 4.2-fold enhancement (–60 mV relative to –90 mV). In contrast, robust voltage dependence was not observed for Nav1.8.

### Use Dependence

To model the accumulation of inactivated Navs during periods of high-frequency action potentials, we investigated the use-dependent block of sodium current by vixotrigine. From a holding potential of –60 mV, we applied a train of 25 depolarizing voltage steps (20 milliseconds to +10 mV) at 10 Hz (100-millisecond start-start interval) (Fig. 2A). As expected, this voltage step protocol resulted in a use-dependent reduction of sodium current. Relative to the first pulse, we found 25%–83% of the sodium current was evoked at the final (25th) pulse: 35.1% for Nav1.1, 58.6% for Nav1.2, 68.5% for Nav1.3, 63.9% for Nav1.4, 64.5% for Nav1.5, 75% for Nav1.6, 53.9% for Nav1.7, and 83.7% for Nav1.8 (Fig. 2B). Use-dependent block was calculated from the current evoked by the final voltage pulse in the 25-pulse train, normalized to the drug-free baseline. We found a shift toward increased potency in all Nav subtypes, averaging a 3.95-fold change in $IC_{50}$ (Fig. 2C). For example, the $IC_{50}$ of vixotrigine shifted from 6.11 to 1.76 μM for the final test pulse, blocking nearly 35% of the baseline Nav1.7 peak current at 1 μM. The $IC_{50}$ shift between the first and final depolarizing pulses ranged from 2.6- to 6-fold, with the largest shifts observed for Nav1.2.

### Selectivity

To assess selectivity across a panel of Navs, we benchmarked vixotrigine to the broad-spectrum Nav blocker, carbamazepine; PF-05089771, a Nav1.7 blocker; and A-803467,

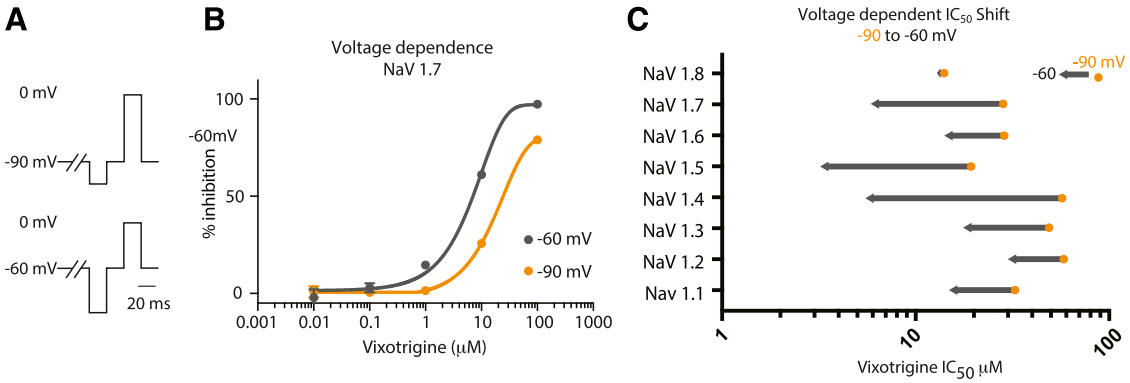


**Fig. 1.** Vixotrigine is a voltage-dependent Nav blocker. (A) Voltage protocols to investigate voltage-dependent inhibition of Nav1.x subtypes. Holding potentials were –90 and –60 mV (or –90 and –70 mV for Nav1.5). A conditioning prepulse to –120 mV was applied 20 milliseconds prior to test pulses to 0 or 10 mV. Peak currents were measured during the 20-millisecond test pulse. (B) Vixotrigine inhibition of Nav1.7 is dependent on holding potential. The concentration-response relationship shifts left at depolarized potentials (–60 mV) relative to –90 mV. Values are means ± S.D. for all wells recorded at each concentration ($n$ = 4–6 wells/concentration). (C) Plot of voltage-dependent $IC_{50}$ shifts for Nav1.1–1.8. Orange points are $IC_{50}$ values for holding potentials of –90 mV. Arrowheads indicate $IC_{50}$ values for holding potentials of –60 or –70 mV. A decrease in $IC_{50}$ concentration was seen for Nav1.1–1.7.

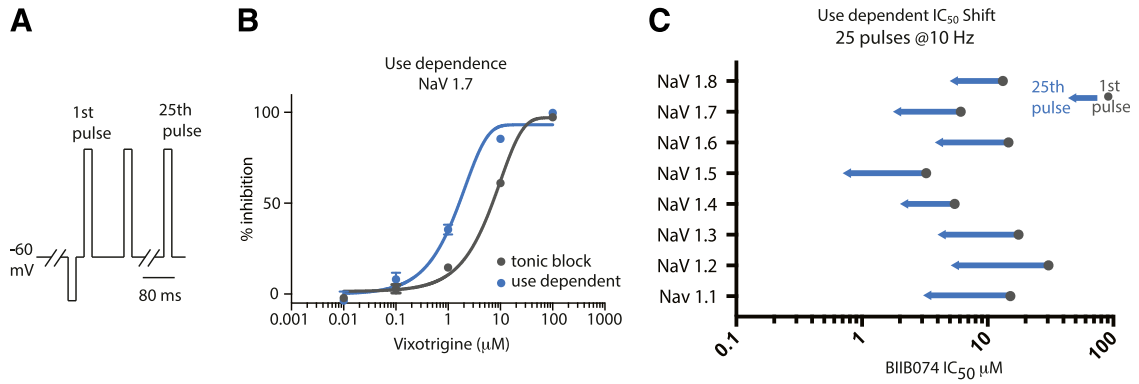


**Fig. 2.** Vixotrigine is a use-dependent Nav blocker. (A) Voltage protocols to demonstrate use-dependent inhibition of Nav1.x. From a holding potential of –60 mV (–70 mV for Nav1.5), a series of 25 depolarizing steps at 10 Hz evoked sodium currents. The peak amplitude of the 25th pulse was used to calculate use-dependent block. (B) Vixotrigine inhibition of Nav1.7 is use-dependent. The concentration-response curve for vixotrigine shifts left for the 25th pulse (blue) relative to the first pulse (gray). Values are means ± S.D. for all wells recorded at each concentration ($n$ = 4–6 wells/concentration). (C) Plot of use-dependent $IC_{50}$ shifts for Nav1.1–1.8, with the same format as Fig. 1B. Vixotrigine use-dependent $IC_{50}$ values decreased for all Nav subtypes.

a Nav1.8 blocker (Jarvis et al., 2007; Alexandrou et al., 2016). To compare selectivity profiles, we first plotted concentration-response curves for each compound's inhibition of peak Nav current for two voltage protocols: tonic block from a holding potential of –60 mV (–70 mV for Nav1.5) and the use-dependent block from –60 mV (25th pulse at 10 Hz) (Fig. 3A). Across all Nav subtypes, we found that $IC_{50}$ values for vixotrigine were within one log unit for both protocols and that vixotrigine reached >90% inhibition of all Nav subtypes at 100 μM, reflecting a potent block of all tested Nav subtypes in this paradigm.

Carbamazepine inhibited a spectrum of Navs, including the DRG-enriched Nav1.7. Compared with vixotrigine, both tonic- and use-dependent carbamazepine antagonism was significantly less potent. For Nav1.3, 1.4, 1.5, and 1.7, $IC_{50}$ values were 86.74, 45.76, 22.92, and 46.72 μM, respectively (use-dependent $IC_{50}$ values from –60 mV) (Fig. 3B). Because 100 μM carbamazepine failed to reach 50% current inhibition

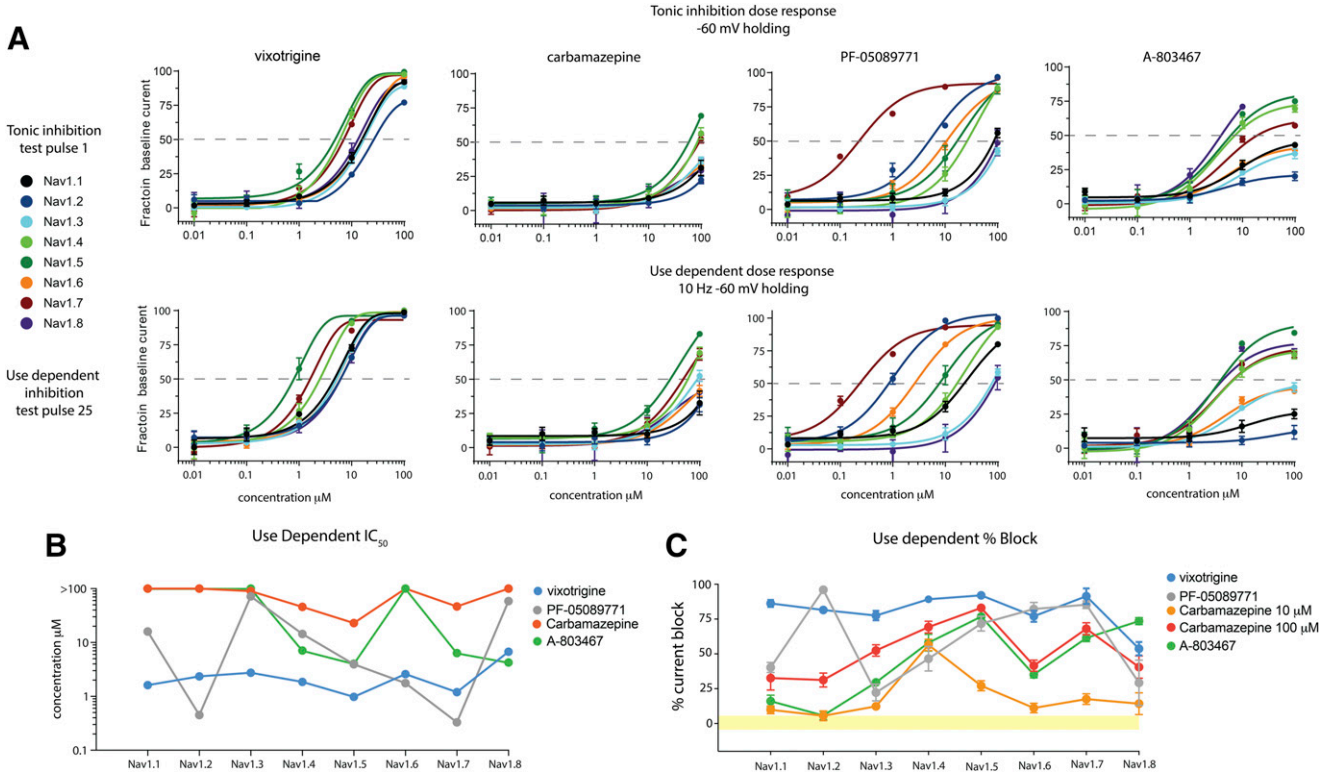


**Fig. 3.** Nav selectivity profiles for vixotrigine, carbamazepine, PF-05089771, and A-803467. (A) Five-point concentration-response curves for tonic block at –60 mV (–70 mV Nav1.5), top panels; use-dependent block (25th pulse at 10 Hz from –60 mV), lower panels. All compounds were compared over the same concentration range for human Nav1.1–1.8. Points are means ± S.D. for all wells recorded at each concentration ($n$ = 4–6 wells/concentration for each drug). (B) Use-dependent Nav1.1–1.8 $IC_{50}$ values for each compound that is presented in (A). $IC_{50}$ values (<50% block) beyond the concentration range are plotted at >100 on the $y$-axis. Vixotrigine Nav1.1–1.8 $IC_{50}$ values are within one log unit, whereas PF-05086771 shows both sub-micromolar and out-of-range $IC_{50}$ values. (C) Use-dependent Nav1.1–1.8 percent peak current blocked at 10 μM for vixotrigine, PF-05089771, A-803467, and at 100 μM for carbamazepine. Yellow line denotes ±5% peak current block.

for Nav1.1, 1.2, 1.6, and 1.8, we plotted the percentage of the current blocked by carbamazepine (Fig. 3C). At 100 μM we found that 31%–83% of the current was blocked (maximum inhibition of 32.6% for Nav1.1, 31.3% for Nav1.2, 41.5% for Nav1.6, and 40.5% for Nav1.8). Although these results show differences in potency across the panel of Nav subtypes, when defined, $IC_{50}$ values varied <4-fold, whereas the remaining Nav subtypes were inhibited to a similar degree with 100 μM carbamazepine. Consistent with published reports, we found evidence for carbamazepine state-dependent block, with an average 1.9-fold increase in potency in our use-dependent protocol. Taken together, these results suggest that vixotrigine, compared with carbamazepine (a clinically relevant broad-spectrum Nav blocker), shows increased potency and enhanced state-dependent block. A summary of tonic and use-dependent $IC_{50}$ values are presented in Supplemental Table 2.

To assess whether our assays could recapitulate reported Nav subtype specificity, we tested PF-05089771 and A-803467, which are reported Nav1.7 and 1.8 blockers, respectively (Jarvis et al., 2007; Alexandrou et al., 2016). In agreement with published data (Alexandrou et al., 2016), PF-05089771 most potently inhibited Nav1.7. Depending on the voltage protocol, we found an ~3- to ~17-fold selectivity over Nav1.2, the next most potently inhibited channel (–60 mV holding; use-dependent difference ~3-fold, tonic difference ~17-fold) (Fig. 3, A and B). Although we found evidence for a voltage-dependent mechanism of action for PF-05089771 (6.4-fold reduction in Nav1.7 $IC_{50}$ between –90 and –60 mV), we found no further use-dependent shift in $IC_{50}$ for this compound for Nav1.7, potentially reflecting the reported slow kinetics of this compound's Nav1.7 interaction (Theile et al., 2016). Intriguingly, however, we identified a large use-dependent shift in PF-05089771 against Nav1.2 and, to a lesser extent, Nav1.6. This discrepancy was not accounted for by differences in channel availability, as Nav1.2 and 1.7 currents were similarly attenuated during the use-dependent protocol (58.6% and 53.9%, respectively). We found that A-803467 most potently inhibited Nav1.8 from depolarized potentials; however, there was little selectivity over other Nav isoforms, with $IC_{50}$ values varying <2-fold between Nav1.4, 1.5, and 1.8. In contrast, from hyperpolarized potentials, A-803467 exhibited a striking selectivity profile, with an $IC_{50}$ value of 2.3 μM for Nav1.8; all remaining Nav isoforms were inhibited by <35% of their peak amplitude at concentrations up to 100 μM ($IC_{50}$ undefined), suggesting at least a 50-fold difference in potency.

As confirmation of the vixotrigine selectivity profile, we ran a parallel set of high-throughput patch-clamp recordings with the SyncroPatch 384 system (SP384PE). We found a similarly broad profile for vixotrigine inhibition, with a slight decrease in $IC_{50}$ values (Supplemental Fig. 1). Overall, $IC_{50}$ values were within 1 μM for Nav1.4, 1.5, and 1.7. This suggests that our conclusions are robust across recording configurations and not artifacts of the perforated patch configuration. Together, these independent experiments confirm that our assay conditions can detect Nav subtype–selective inhibition and suggest that vixotrigine is a broad-spectrum Nav inhibitor.

To assess our ability to validate vixotrigine and carbamazepine in rodent nociceptor models, we expressed rat Nav1.7 in HEK and Nav 1.8 in CHO cells. When evaluated for voltage and use dependence against these recombinant channels, we found a similar profile to the human analogs, in which $IC_{50}$ values for vixotrigine varied ~2-fold between rodent and mouse channels in comparable voltage protocols. For carbamazepine, we found increased potency against rat Nav1.7 and 1.8, with similar trends for state-dependent inhibition. These results suggest that experiments in rodent models will reflect a similar mechanism of action on native Navs as those in recombinant human channels (Supplemental Fig. 2).

**Modulation of Slow- and Fast-Inactivation Onset.** Previous studies have differentiated clinically relevant broad-spectrum Nav blockers, such as carbamazepine and lacosamide, based on their kinetics and/or preference for the fast- and slow-inactivated states of Navs, respectively (Niespodziany et al., 2013; Jo and Bean, 2017). Therefore, we conducted a set of studies to examine vixotrigine block, with voltage protocols designed to examine slow- and fast-inactivated Nav states of Nav1.1, 1.2, 1.6, and 1.7, a mixture of CNS and PNS Nav subtypes.

First, we examined the development of slow inactivation by varying the length of 0-mV depolarizing conditioning pulses (Fig. 4A). In drug-free (vehicle) conditions, we found qualitatively similar activity profiles across tested Nav subtypes. For conditioning pulses up to 320 milliseconds, we detected ≥90% recovery (relative to the shortest conditioning pulse) of the sodium current after 5-millisecond recovery pulses of –120 mV, suggesting these conditioning pulses primarily generated fast-inactivated channel states (Fig. 4B). As expected, increasing the length of conditioning pulses to ≥1 second generated a large reduction in available sodium current after a 5-millisecond recovery pulse to relieve fast inactivation (Fig. 4B), which is indicative of a large fraction of slow-inactivated channels after long conditioning pulses.

To examine the pharmacological interactions with the slow-inactivated channel states, we focused on high compound concentrations, analyzing the highest compound concentration available without visible precipitation from the recording buffer; this approach facilitated comparisons between compounds with distinct properties. In cells exposed to 300 μM carbamazepine, we found a steep drop-off in the available sodium current that preceded the onset of slow inactivation, followed by a relatively shallow plateau between 100 and 1000 milliseconds, which is consistent with previous descriptions of carbamazepine block of fast-inactivated channels and similar to the kinetic profile observed with 300 μM lamotrigine (Sheets et al., 2008) (Fig. 4C). In contrast, the time course of lacosamide block was shifted toward longer depolarizations. Relative to carbamazepine, we detected significantly less sodium current inhibition by lacosamide (1000 μM) until conditioning pulses reached durations of >1000 milliseconds. Finally, in the presence of 100 μM vixotrigine, we found a steep drop-off in the available sodium current, which reached a plateau after ~100-millisecond conditioning pulses. Therefore, the majority of vixotrigine Nav block occurred before the onset of significant slow inactivation.

To facilitate the comparison of compound block kinetics, we plotted Nav current inhibition relative to the time-dependent decrease in vehicle conditions. The minima of these curves represent the most pronounced Nav inhibition relative to vehicle (Fig. 4D). For vixotrigine (100 μM), the maximal inhibition occurred between 80- and 160-millisecond inactivation pulse durations (Nav1.1, 1.2, 1.6, and 1.7), which is

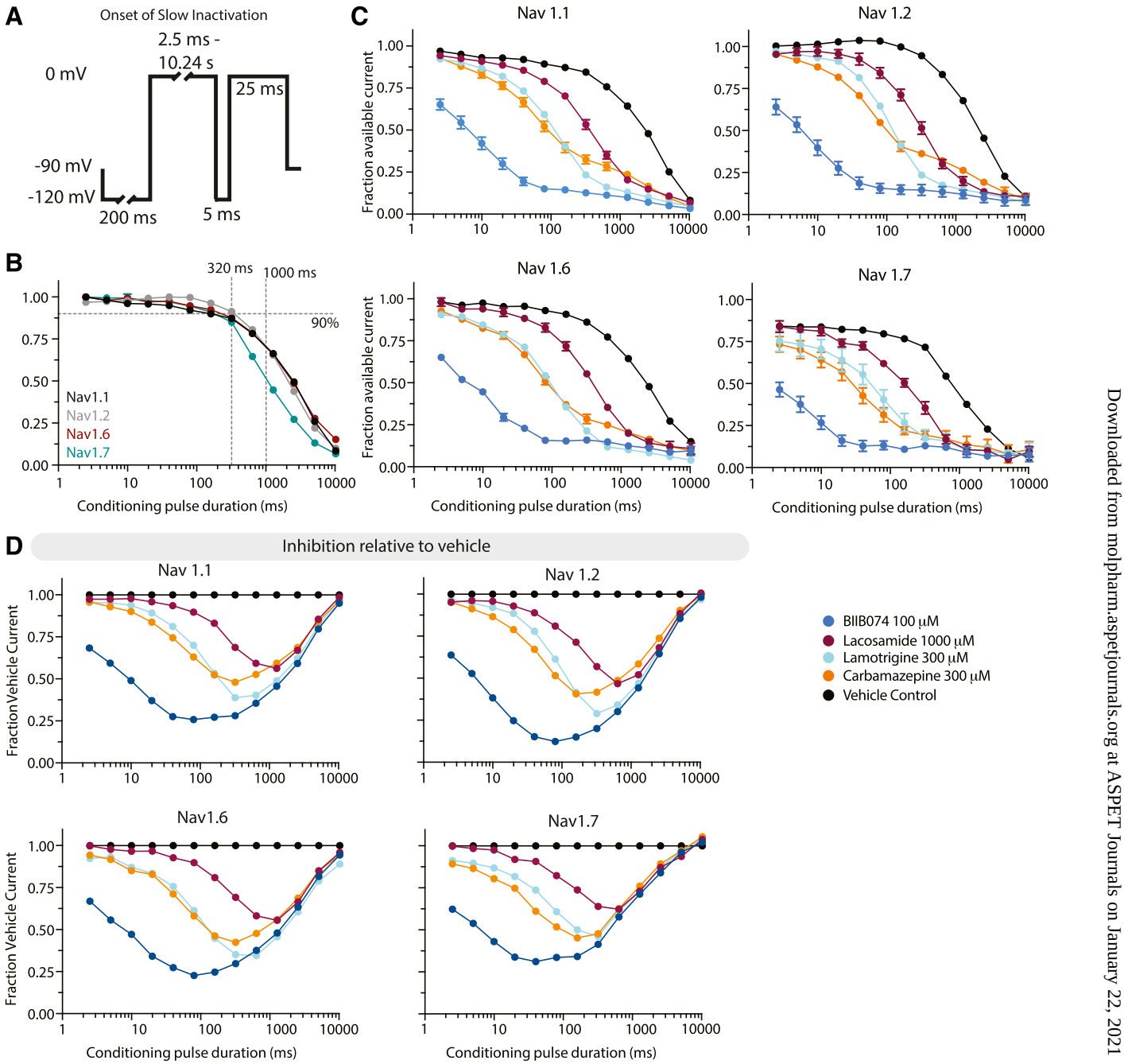


**Fig. 4.** Onset of slow-inactivation states and block by vixotrigine, lacosamide, lamotrigine, and carbamazepine. (A) Voltage protocol to examine slow inactivation. Variable lengths of 0-mV depolarizing pulses followed by a 5-millisecond recovery pulse to relieve fast inactivation. (B) Plot of conditioning pulse duration vs. channel availability relative to 2.5-millisecond conditioning pulses. Each Nav subtype shows similar time-dependent onset of slow inactivation, with a large loss of channel availability after 1-second conditioning pulses. (C) Channel availability vs. conditioning pulse duration for Nav1.1, 1.2, 1.6, and 1.7 in the presence of Nav blockers. Black curves show channel availability in vehicle. Vixotrigine, carbamazepine, and lamotrigine block occurs before significant slow inactivation. Lacosamide block develops after depolarizations >320 milliseconds. (D) Data from (C) plotted as difference relative to vehicle channel availability at each conditioning pulse duration. Curve minima are the times with the largest differences relative to vehicle. Points are means ± S.D. for all wells tested at each concentration ($n$ = 4–10 wells/condition).

similar to the 160- to 320-millisecond peaks observed for 300 μM carbamazepine and lamotrigine. In contrast, 1000 μM lacosamide reached its peak difference, relative to vehicle, between 640 and 1280 milliseconds. At lower compound concentrations, these peak times shifted toward longer values, but the relative pattern between compounds was retained (data not shown). Based on these experiments, we conclude that vixotrigine channel block develops before the onset of slow inactivation, consistent with inhibition of fast-inactivated channel states.

**Vixotrigine Slows Recovery from Inactivation.** Next, we examined whether vixotrigine modulated the time course of inactivation recovery. To probe the interaction with slow-inactivated states, we varied recovery time after 1-second, 0-mV conditioning pulses (Fig. 5A). We used 1-second depolarizing pulses as a compromise between cell/recording quality

and the development of sufficient slow inactivation (Fig. 4B). Using this protocol, we found that Nav current amplitude recovered to ~90% of control values after 1-second recovery times, suggesting these parameters are sufficient to investigate recovery from slow inactivation (Fig. 5B).

Similar to the development of slow inactivation, we found that recovery from slow inactivation proceeded quickly in the presence of carbamazepine, reaching vehicle control levels after ~40-millisecond recovery times, for which recovery from slow inactivation is minimal (Fig. 5C). We found that, in the presence of lacosamide, Nav current recovered to vehicle values after 320- to 640-millisecond recovery times, which is an ~10-fold shift relative to carbamazepine. In this voltage paradigm, lamotrigine kinetics were between those of carbamazepine and lacosamide. Although the onset of vixotrigine block was rapid (Fig. 4C), when examining the recovery kinetics, we found a significant prolongation of recovery, similar to lacosamide. Recovery from vixotrigine block to vehicle control levels required recovery times of ~640 milliseconds. These recordings suggest that although vixotrigine rapidly inhibits Nav currents, like carbamazepine, it slows recovery from the inactivated state, which is superficially similar to lacosamide. Therefore, we asked whether vixotrigine prolongs recovery from fast-inactivated states.

We induced fast inactivation with a 10-millisecond, 0-mV conditioning pulse, followed by variable lengths of hyperpolarizing recovery pulses (Fig. 6A). Consistent with the selective generation of fast-inactivated states, in vehicle, sodium currents recovered to baseline values rapidly, reaching 100% of the available current, with 10- to 20-millisecond recovery times (Fig. 6B). Using this protocol, we observed a significant prolongation of Nav recovery in the presence of vixotrigine, with a time course similar to that observed for the recovery from slow inactivation, requiring ~640-millisecond recovery times to reach vehicle control (Fig. 6C). Notably, with this protocol, the magnitude of inhibition detected for carbamazepine was significantly reduced relative to vixotrigine, potentially revealing differences in carbamazepine and vixotrigine binding kinetics. As expected, we found minimal inhibition of any Nav subtype by 1000 μM lacosamide, which is consistent with slow-inactivation preference and/or slow association kinetics. Taken together, these results recapitulate expected kinetic profiles of carbamazepine and lacosamide while mechanistically distinguishing vixotrigine from these clinically relevant Nav blocker compounds.

### Inhibition of Sensory Neuron Sodium Currents

To examine the effects of vixotrigine on native sensory neuron sodium channels, we measured the impact of vixotrigine on sodium currents in dissociated rat DRG neurons. We enriched our data set for small-diameter DRG cells by selecting neurons <25 μM for recording (mean 20.5 ± 2.9 μM). We found that 10 μM vixotrigine did not significantly alter steady-state activation curves relative to vehicle control (–120 mV prepulse, not shown). Furthermore, we found no statistically significant impact on the maximum evoked current amplitude when sodium channels were conditioned with hyperpolarized voltage prepulses (negative to –95 mV). In contrast, we found a left shift in the steady-state inactivation curves in the presence of 10 μM vixotrigine. After 1-second voltage prepulses between –95 and –35 mV, we found a significant reduction in the maximum evoked sodium current, reflecting a voltage-dependent block of native DRG Navs. At a 100 μM concentration, carbamazepine shifted the steady-state inactivation curve over a similar range and



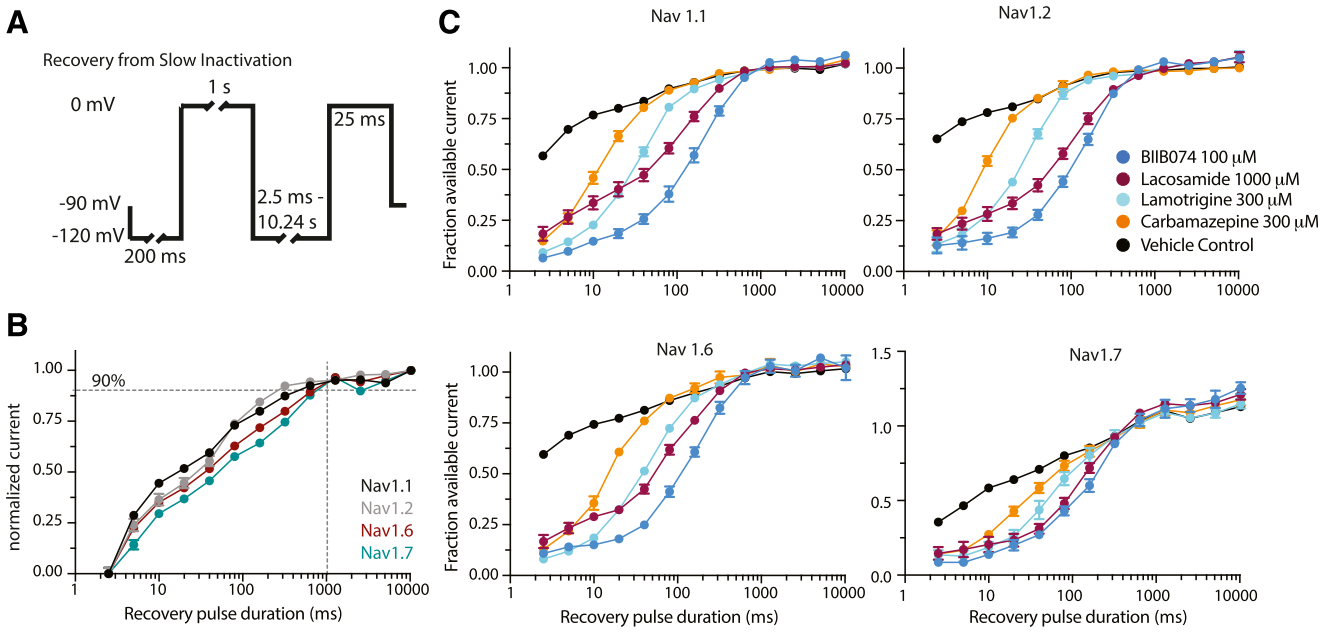


**Fig. 5.** Recovery from slow inactivation. (A) Voltage protocol to examine recovery from slow inactivation. Slow inactivation was induced with 1-second, 0-mV conditioning pulses followed by variable hyperpolarizing recovery times. (B) Comparison of slow-inactivation recovery kinetics for Nav subtypes. Nav availability recovers to >90% after 1-second recovery pulses. (C) Pharmacological modulation of slow-inactivation recovery. Channel availability plotted as a function of recovery pulse duration for Nav1.1, 1.2, 1.6, and 1.7. Vixotrigine prolongs recovery from slow inactivation similarly to lacosamide, whereas carbamazepine block recovers to baseline within ~100 milliseconds. Points are means ± S.D. for all wells tested at each concentration ($n$ = 4–11 wells/condition).

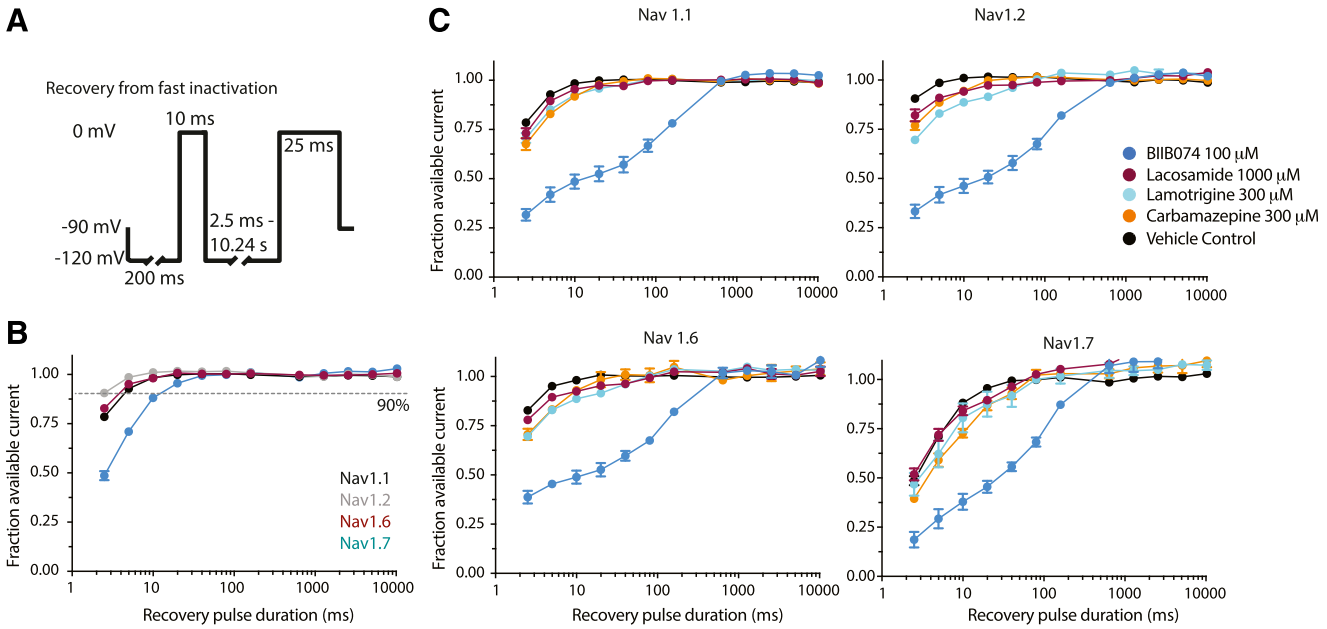


**Fig. 6.** Recovery from fast inactivation. (A) Voltage protocol to examine recovery from fast inactivation. Fast inactivation was induced with 10-millisecond, 0-mV conditioning pulses followed by variable hyperpolarizing recovery times. (B) Comparison of fast-inactivation recovery kinetics for Nav subtypes. Nav availability recovers to >90% after 10- to 40-millisecond recovery pulses. (C) Pharmacological modulation of slow-inactivation recovery. Channel availability plotted as a function of recovery pulse duration for Nav1.1, 1.2, 1.6, and 1.7. Vixotrigine prolongs recovery from fast inactivation similarly to slow inactivation. Points are means ± S.D. for all wells tested at each concentration ($n$ = 4–11 wells/condition).

magnitude to vixotrigine (Figs. 4B; Fig. 7, A and B). In contrast, we did not find a shift in the steady-state inactivation curve with 11 μM carbamazepine (Fig. 7C). Therefore, although carbamazepine and vixotrigine have similar effects on DRG sodium current inactivation profiles, their potencies are separated by an order of magnitude.

## Discussion

Here, we report the first systematic Nav selectivity and mechanism-of-action data set for vixotrigine. Using well validated cell lines, comparable voltage protocols, and multiple experimental platforms, we provide evidence that vixotrigine is a broad-spectrum, state-dependent sodium channel blocker that slows the recovery of inactivated channels. Taken together, these voltage- and use-dependent recording paradigms suggest that vixotrigine acts with a similar mechanism regardless of Nav subtype and will preferentially target inactivated sodium channels in depolarized and/or hyperactive neurons.

Previous summaries of vixotrigine have offered few specific data regarding Nav subtype selectivity. A recent commentary on this molecule, based on the limited publicly available information, suggested that it has been investigated as a blocker for multiple Nav subtypes (Hesselink, 2017). Most recently, vixotrigine was reported as a Nav1.7-selective, state-dependent blocker, but peer-reviewed data quantifying selectivity were not published (Zakrzewska et al., 2017). In contrast, a voltage-imaging study reported a broad spectrum of Nav inhibition with vixotrigine after chemical stimulation

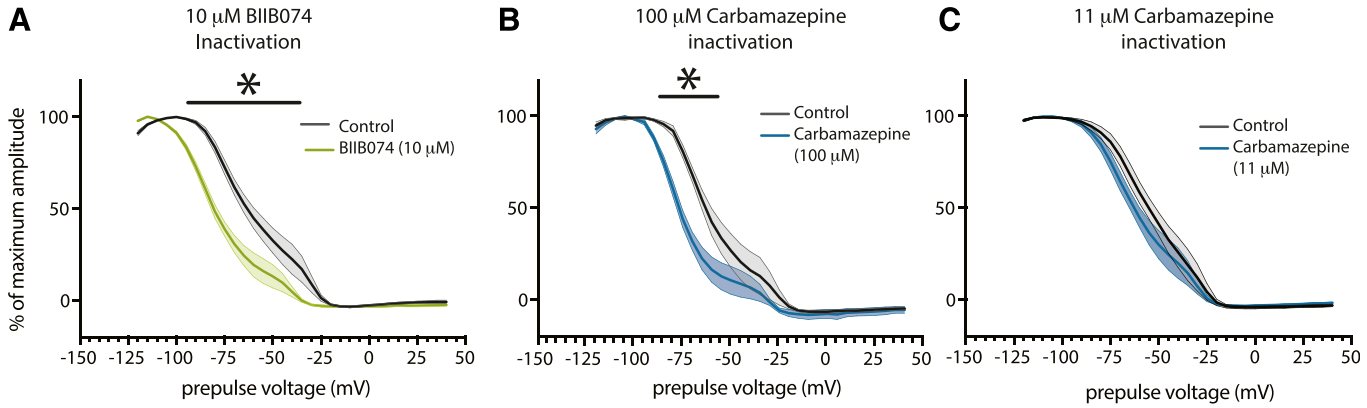


**Fig. 7.** Vixotrigine effect on DRG neuron sodium currents. (A) Vixotrigine shifts steady-state sodium current inactivation curves left at 10 μM. Significant differences from control were found after test pulses between –95 and –35 mV ($n$ = 8 neurons vehicle, $n$ = 8 vixotrigine). (B) Carbamazepine shifts steady-state sodium inactivation curves left at 100 μM ($n$ = 5). Significant differences from control were found between –85 and –55 mV. (C) Carbamazepine did not significantly shift DRG inactivation curves relative to control at 11 μM ($n$ = 9). Asterisk denotes voltage range significanlty different from control $p<0.05$.

of Navs in a recombinant HEK system (Deuis et al., 2016). Although reports of subtype selectivity have been contradictory, studies by two independent groups have reported state-dependent inhibition of Nav1.7 by vixotrigine (Zheng et al., 2018).

The experiments presented here were designed to robustly examine the relative potencies and mechanism of action of vixotrigine and subtype-specific and subtype-nonspecific reference compounds across Nav1.1 to 1.8 under idealized conditions. Based on these data, we conclude that vixotrigine is a broad-spectrum Nav blocker, with $IC_{50}$ values varying <10-fold across the different subtypes. Our data also demonstrate that vixotrigine has strong efficacy for inhibiting peak sodium current, reaching >90% block across all Nav subtypes studied.

Because absolute $IC_{50}$ values are difficult to compare between studies—as a result of biologic (cell lines), technical (recording platform), and neurophysiological (specific voltage protocols) variables—we directly compared vixotrigine action across a panel of Nav subtypes and benchmarked our assessment of selectivity to previously reported subtype-selective compounds. Our data paint a complex picture of PF-05089771 and A-803467 (Jarvis et al., 2007; Alexandrou et al., 2016) selectivity, with significant differences based on the specific voltage- and use-dependent paradigms. Nonetheless, consistent with published data, our recordings find clear Nav selectivity profiles for these compounds, in contrast with vixotrigine.

Similar to subtype selectivity, state-dependent properties will effectively bias compound action away from hyperpolarized tissues, such as cardiac muscle, and toward pathologically hyperactive neuronal populations. In both voltage- and use-dependent paradigms, we detected an ~4-fold increase in potency for vixotrigine, reflecting its preferential block of inactivated channels. Importantly, our voltage-dependent protocols were intended to provide perspective on state dependence within a normal physiologic range of membrane potentials, with –90 mV reflecting skeletal and heart muscle and –60 mV for neuronal membrane potential. Larger voltage-dependent shifts in $IC_{50}$ would likely be reported for vixotrigine by comparing full activation voltages (i.e., –120 mV) with an empirically determined half-maximal voltage for each channel subtype. Likewise, use-dependent $IC_{50}$ shifts are products of specific voltage protocols. Here, we report a 10-Hz use-dependent block for all Nav1.1–1.7 subtypes. This approach allows clear investigation of mechanism of action and selectivity between Nav types under similar conditions, bolstering our understanding of a broad-spectrum use dependence. As a consequence, these use-dependent $IC_{50}$ values do not equally reflect distinct effects on physiologic firing rates for cell types such as cortical interneurons and cardiomyocytes.

Our identification of a clear state-dependent block for all Nav subtypes indicates that the effective potency of vixotrigine will vary depending on the physiologic (or pathophysiological) activity of the tissue. For example, with Nav1.5, we find a ~25-fold increase in vixotrigine potency between hyperpolarized potentials and our use-dependent measurement ($IC_{50}$ 18.65 vs. 0.74 μM, respectively). Because our use-dependent protocol does not reflect physiologic human cardiac muscle activity, this protocol confirms the state-dependent interaction of vixotrigine with Nav1.5, whereas the potency from hyperpolarized potentials more closely approximates a physiologic context.

Orally administered nonspecific Nav inhibitors are approved in neuropathic pain and as anticonvulsants; specifically, carbamazepine is approved by the FDA for the treatment of trigeminal neuralgia, lacosamide is approved by the FDA for partial-onset seizures, and lamotrigine is approved by the FDA for epilepsy [see also (Cruccu et al., 2008); (Wiffen et al., 2011; Lattanzi et al., 2015; Nevitt et al., 2018)]. Here, we compare these compounds as exemplars of clinically relevant but mechanistically distinct Nav blockers. Our results confirm that carbamazepine is a broadly acting inhibitor of CNS, cardiac muscle, skeletal muscle, and PNS Nav subtypes. Notably, we provide evidence for a prominent block of Nav1.4 and 1.5 relative to neural Nav subtypes and a moderate, approximately 2-fold increase in use-dependent potency. Overall, we found that vixotrigine was significantly more potent than carbamazepine. For example, vixotrigine use-dependent Nav1.7 $IC_{50}$ values were 25-fold more potent than carbamazepine. We found similar results with native DRG sodium currents, in which vixotrigine and carbamazepine had a similar effect on steady-state inactivation but with a 10-fold difference in potency. These results are in agreement with those reported by Zheng et al. (2018), in which vixotrigine shifted Nav1.7 steady-state inactivation but did not alter channel activation.

In addition to the canonical voltage and use state dependences, Nav blockers may be further characterized by their preference for fast- or slow-inactivation channel states and/or their binding/dissociation kinetics from the inactivated channel (Karoly et al., 2010). For example, carbamazepine, lacosamide, and lamotrigine have been described as having preference for the fast- and slow-inactivation states and/or fast and slow kinetics (Sheets et al., 2008; Qiao et al., 2014). Our data recapitulate these results, demonstrating a rapid Nav block and recovery in the presence of carbamazepine, whereas lacosamide inhibition requires prolonged depolarizations and recovery times to generate and recover from block. With vixotrigine, our data expand on a previous characterization (Zheng et al., 2018), providing context through our contemporaneous characterization of multiple Nav subtypes and clinically relevant Nav blocker activity profiles. We identify a rapid onset of vixotrigine block, suggesting that effects occur through fast-inactivated channels. When examined in the context of slow inactivation, vixotrigine slows Nav recovery to a similar degree as lacosamide; however, fast-inactivated channel states are sufficient to describe the recovery time course. Notably, similar kinetic profiles for block and recovery have been described for local anesthetics such as lidocaine, another class of broad-spectrum Nav blocker (Gawali et al., 2015).

How these activity profiles map onto clinical efficacy is unknown; however, it has been reported that carbamazepine is effective in patients with Nav1.7 mutations that lead to painful neuropathy (Adi et al., 2018). Experiments in recombinant systems suggest carbamazepine affects these mutant channels by modulating inactivation as opposed to restoring normal channel activation. Likewise, a recent study identified a striking correlation between lacosamide modulation of Nav1.7 mutation channels in patients and clinical efficacy (Labau et al., 2020). These observations suggest that the underlying molecular driver of pathologic neural activity may

constrain the efficacy of Nav blockers based on their particular mechanism of action. Although further studies will be required to validate the effect of vixotrigine on specific Nav mutants, these observations suggest translatability between modulation of Nav properties in recombinant systems and clinical efficacy. Vixotrigine has shown promise clinically in trigeminal neuralgia, with significant improvements in secondary trial endpoints reported (Zakrzewska et al., 2017). Improvement in neuropathic pain was also observed in a phase 2 study of participants with painful lumbosacral radiculopathy, but a larger follow-up study did not confirm the results (Versavel, 2015; Forrestal et al., 2019). Vixotrigine is currently under investigation in neuropathic pain; a phase 2 study in small fiber neuropathy is ongoing (clinicaltrials.gov/ct2/show/NCT03339336).

In conclusion, we show that vixotrigine is a broad-spectrum, voltage- and use-dependent Nav blocker. Mechanistically, vixotrigine blocks fast-inactivated channels and slows channel recovery from inactivated states. Vixotrigine remains under investigation for neuropathic pain. The combination of broad-spectrum Nav block, state dependence, and block kinetics suggests potential for vixotrigine efficacy in a variety of PNS and CNS disorders.

#### Acknowledgments

Biogen provided funding for medical writing support in the development of this paper, Yien Liu (Excel Scientific Solutions, Southport, CT) contributed to the first draft of the manuscript based on input from the authors, and Miranda Dixon (Excel Scientific Solutions, Horsham, UK) copyedited and styled the manuscript per journal requirements. Biogen reviewed and provided feedback on the manuscript. The authors had full editorial control of the manuscript and provided their final approval of all content.

#### Authorship Contributions

*Participated in research design:* Hinckley, Naik, Hajos.

*Conducted experiments:* Kuryshev, Sers, Barre, Buisson.

*Performed data analysis:* Hinckley, Kuryshev, Sers, Barre.

*Wrote or contributed to the writing of the manuscript:* Hinckley, Kuryshev, Sers, Barre, Buisson, Naik, Hajos.

#### References

Adi T, Estacion M, Schulman BR, Vernino S, Dib-Hajj SD, and Waxman SG (2018) A novel gain-of-function $Na_v1.7$ mutation in a carbamazepine-responsive patient with adult-onset painful peripheral neuropathy. *Mol Pain* **14**:1744806918815007.

Alexandrou AJ, Brown AR, Chapman ML, Estacion M, Turner J, Mis MA, Wilbrey A, Payne EC, Gutteridge A, Cox PJ, et al. (2016) Subtype-selective small molecule inhibitors reveal a fundamental role for Nav1. 7 in nociceptor electrogenesis, axonal conduction and presynaptic release. *PLoS One* **11**:e0152405.

Bennett DL, Clark AJ, Huang J, Waxman SG, and Dib-Hajj SD (2019) The role of voltage-gated sodium channels in pain signaling. *Physiol Rev* **99**:1079–1151.

Boucher TJ, Okuse K, Bennett DL, Munson JB, Wood JN, and McMahon SB (2000) Potent analgesic effects of GDNF in neuropathic pain states. *Science* **290**:124–127.

Cruccu G, Gronseth G, Alksne J, Argoff C, Brainin M, Burchiel K, Nurmikko T, and Zakrzewska JM; American Academy of Neurology Society; European Federation of Neurological Society (2008) AAN-EFNS guidelines on trigeminal neuralgia management. *Eur J Neurol* **15**:1013–1028.

Cummins TR, Dib-Hajj SD, and Waxman SG (2004) Electrophysiological properties of mutant Nav1.7 sodium channels in a painful inherited neuropathy. *J Neurosci* **24**:8232–8236.

Deuis JR, Wingerd JS, Winter Z, Durek T, Dekan Z, Sousa SR, Zimmermann K, Hoffmann T, Weidner C, Nassar MA, et al. (2016) Analgesic effects of GpTx-1, PF-04856264 and CNV1014802 in a mouse model of NaV1.7-mediated pain. *Toxins (Basel)* **8**:78.

Forrestal F, Naik H, Shinobu L, et al. (2019, May 9-11;) Assessment of the efficacy and safety of vixotrigine in participants with lumbosacral radiculopathy: results of a randomized, placebo-controlled trial [PS02]. *Presented at: 7th International Congress on Neuropathic Pain* **London, UK** (London, UK).

Gawali VS, Lukacs P, Cervenka R, Koenig X, Rubi L, Hilber K, Sandtner W, and Todt H (2015) Mechanism of modification, by lidocaine, of fast and slow recovery from inactivation of voltage-gated $Na^+$ channels. *Mol Pharmacol* **88**:866–879.

He X-H, Zang Y, Chen X, Pang R-P, Xu J-T, Zhou X, Wei X-H, Li Y-Y, Xin W-J, Qin Z-H, et al. (2010) TNF-$\alpha$ contributes to up-regulation of Nav1.3 and Nav1.8 in DRG neurons following motor fiber injury. *Pain* **151**:266–279.

Hesselink JMK (2017) Moving targets in sodium channel blocker development: the case of raxatrigine: from a central NaV1.3 blocker via a peripheral NaV1.7 blocker to a less selective sodium channel blocker. *J Med Ther* **1**:1–3.

Howell KB, McMahon JM, Carvill GL, Tambunan D, Mackay MT, Rodriguez-Casero V, Webster R, Clark D, Freeman JL, Calvert S, et al. (2015) SCN2A encephalopathy: a major cause of epilepsy of infancy with migrating focal seizures. *Neurology* **85**:958–966.

Ichikawa K, Koyama N, Kiguchi S, Kojima M, and Yokota T (2001) Inhibitory effect of oxcarbazepine on high-frequency firing in peripheral nerve fibers. *Eur J Pharmacol* **420**:119–122.

Jarvis MF, Honore P, Shieh CC, Chapman M, Joshi S, Zhang XF, Kort M, Carroll W, Marron B, Atkinson R, et al. (2007) A-803467, a potent and selective Nav1.8 sodium channel blocker, attenuates neuropathic and inflammatory pain in the rat. *Proc Natl Acad Sci USA* **104**:8520–8525.

Jo S and Bean BP (2017) Lacosamide inhibition of Nav1.7 voltage-gated sodium channels: slow binding to fast-inactivated states. *Mol Pharmacol* **91**:277–286.

Karoly R, Lenkey N, Juhasz AO, Vizi ES, and Mike A (2010) Fast- or slow-inactivated state preference of Na+ channel inhibitors: a simulation and experimental study. *PLOS Comput Biol* **6**:e1000818.

Labau JIR, Estacion M, Tanaka BS, de Greef BTA, Hoeijmakers JGJ, Geerts M, Gerrits MM, Smeets HJM, Faber CG, Merkies ISJ, et al. (2020) Differential effect of lacosamide on Nav1.7 variants from responsive and non-responsive patients with small fibre neuropathy. *Brain* **143**:771–782.

Lattanzi S, Cagnetti C, Foschi N, Provinciali L, and Silvestrini M (2015) Lacosamide monotherapy for partial onset seizures. *Seizure* **27**:71–74.

Michel MC, Murphy TJ, and Motulsky HJ (2020) New author guidelines for displaying data and reporting data analysis and statistical methods in experimental biology. *J Pharmacol Exp Ther* **372**:136–147.

Nevitt SJ, Tudur Smith C, Weston J, and Marson AG (2018) Lamotrigine versus carbamazepine monotherapy for epilepsy: an individual participant data review. *Cochrane Database Syst Rev* **6**:CD001031.

Niespodziany I, Leclère N, Vandenplas C, Foerch P, and Wolff C (2013) Comparative study of lacosamide and classical sodium channel blocking antiepileptic drugs on sodium channel slow inactivation. *J Neurosci Res* **91**:436–443.

Qiao X, Sun G, Clare JJ, Werkman TR, and Wadman WJ (2014) Properties of human brain sodium channel $\alpha$-subunits expressed in HEK293 cells and their modulation by carbamazepine, phenytoin and lamotrigine. *Br J Pharmacol* **171**:1054–1067.

Sheets PL, Heers C, Stoehr T, and Cummins TR (2008) Differential block of sensory neuronal voltage-gated sodium channels by lacosamide [(2R)-2-(acetylamino)-N-benzyl-3-methoxypropanamide], lidocaine, and carbamazepine. *J Pharmacol Exp Ther* **326**:89–99.

Theile JW, Fuller MD, and Chapman ML (2016) The selective Nav1.7 inhibitor, PF-05089771, interacts equivalently with fast and slow inactivated Nav1.7 channels. *Mol Pharmacol* **90**:540–548.

Veeramah KR, O'Brien JE, Meisler MH, Cheng X, Dib-Hajj SD, Waxman SG, Talwar D, Girirajan S, Eichler EE, Restifo LL, et al. (2012) De novo pathogenic SCN8A mutation identified by whole-genome sequencing of a family quartet affected by infantile epileptic encephalopathy and SUDEP. *Am J Hum Genet* **90**:502–510.

Versavel M (2015) Efficacy and safety of the novel sodium channel blocker CNV1014802 in trigeminal neuralgia and lumbosacral radiculopathy. *J Pain Relief* **4**:36–36.

Waxman SG, Kocsis JD, and Black JA (1994) Type III sodium channel mRNA is expressed in embryonic but not adult spinal sensory neurons, and is reexpressed following axotomy. *J Neurophysiol* **72**:466–470.

Wible BA, Kuryshev YA, Smith SS, Liu Z, and Brown AM (2008) An ion channel library for drug discovery and safety screening on automated platforms. *Assay Drug Dev Technol* **6**:765–780.

Wiffen PJ, Derry S, Moore RA, and McQuay HJ (2011) Carbamazepine for acute and chronic pain in adults. *Cochrane Database Syst Rev*:CD005451.

Wu Y, Ma H, Zhang F, Zhang C, Zou X, and Cao Z (2018) Selective voltage-gated sodium channel peptide toxins from animal venom: pharmacological probes and analgesic drug development. *ACS Chem Neurosci* **9**:187–197.

Yang Y, Wang Y, Li S, Xu Z, Li H, Ma L, Fan J, Bu D, Liu B, Fan Z, et al. (2004) Mutations in SCN9A, encoding a sodium channel alpha subunit, in patients with primary erythermalgia. *J Med Genet* **41**:171–174.

Zakrzewska JM, Palmer J, Morisset V, Giblin GM, Obermann M, Ettlin DA, Cruccu G, Bendtsen L, Estacion M, Derjean D, et al.; study investigators (2017) Safety and efficacy of a Nav1.7 selective sodium channel blocker in patients with trigeminal neuralgia: a double-blind, placebo-controlled, randomised withdrawal phase 2a trial. *Lancet Neurol* **16**:291–300.

Zheng YM, Wang WF, Li YF, Yu Y, and Gao ZB (2018) Enhancing inactivation rather than reducing activation of Nav1.7 channels by a clinically effective analgesic CNV1014802. *Acta Pharmacol Sin* **39**:587–596.

**Address correspondence to:** Dr. Christopher Hinckley, Cellular Physiology Group, Research, Biogen, 115 Broadway, Cambridge, MA 02142. E-mail: chris.hinckley@biogen.com